



# Preparation, characterization and evaluation of a series of heterogeneous platinum catalysts immobilized on magnetic silica with different acid ligands

Laiming Li<sup>1</sup> · Youxin Li<sup>1,2</sup> · Aschenaki Assefa<sup>1</sup> · James J. Bao<sup>1</sup>

Received: 8 May 2019 / Accepted: 31 July 2019 / Published online: 8 August 2019  
© Springer Nature Switzerland AG 2019

## Abstract

Platinum was immobilized on magnetic silica gel by means of boronic, nitric, carboxylic or sulfuric acid ligands to give four heterogeneous Pt nano-catalysts, designated as  $\text{Fe}_3\text{O}_4@ \text{SiO}_2\text{-BA@Pt}$ ,  $\text{Fe}_3\text{O}_4@ \text{SiO}_2\text{-NA@Pt}$ ,  $\text{Fe}_3\text{O}_4@ \text{SiO}_2\text{-CA@Pt}$  and  $\text{Fe}_3\text{O}_4@ \text{SiO}_2\text{-SA@Pt}$ , respectively. Particles of these mono-dispersible Pt catalysts were 10–20 nm in size and could be separated for recycling by means of a magnet.  $\text{Fe}_3\text{O}_4@ \text{SiO}_2\text{-BA@Pt}$  (0.174 mmol/g Pt) showed the best catalytic activity and selectivity, which were better than Speier's catalyst. Its turnover numbers were up to  $1.7 \times 10^6$  and  $1.1 \times 10^6$  for hydrosilylation of 1-hexene or styrene, respectively. This material could also catalyze the hydrosilylation of a broad range of alkenes and alkynes as substrates and methyldichlorosilane or triethoxysilane as silanes. Similar yields of 1-hexyl-methyldichlorosilane at the first and eighth runs (96.5% and 95.2%, respectively), together with a final Pt content of 0.171 mmol/g indicated the outstanding stability of  $\text{Fe}_3\text{O}_4@ \text{SiO}_2\text{-BA@Pt}$  under the catalytic reaction conditions.

## Introduction

Heterogeneous catalysts have several well-known advantages over homogeneous catalysis, including good stability, easy recovery and recycling, and low manufacturing costs [1, 2]. However, their applications in industry remain limited by issues of catalytic efficiency, recycling times and commercial supply [3]. Hence, much effort in catalysis research is directed toward obtaining practical and efficient heterogeneous catalysts [4]. In this context, magnetic nanoparticles have attracted much attention for the immobilization of metal catalysts due to their high stability and useful magnetic properties [5–7]. Magnetic heterogeneous catalysts can often be easily recovered from solution using a magnet, avoiding time- and solvent-consuming recovery procedures.

Thus, magnetic catalysts have much potential in industrial homogeneous catalysis [8]. Magnetic nanoparticles, especially  $\text{Fe}_3\text{O}_4$  encapsulated with silica ( $\text{Fe}_3\text{O}_4@ \text{SiO}_2$ ), are emerging as interesting supports for the immobilization of metal catalysts [9, 10]. In contrast to many traditional supports,  $\text{Fe}_3\text{O}_4@ \text{SiO}_2$  nanoparticles allow for the distribution of active sites throughout the outer surface, which is beneficial for high efficiency in catalytic reactions [11].

Metallic platinum has been widely used as a catalyst in the industrial and laboratory-scale oxidation of toluene, hydrosilylation of alkenes and alkynes, hydrogenolysis of glycerol, decomposition of formaldehyde, sulfuric acid, etc. [12–17]. For example, Karstedt's catalyst and Speier's catalyst can both catalyze hydrosilylation [18]. However, in many cases, the amounts of Pt are low and losses of Pt from the nanoparticles are apparent during recycling, which adversely affect catalytic activity [19, 20]. Thus, there is a requirement for novel and efficient heterogeneous catalysts which can obtain comparable activities and selectivities to homogeneous Pt catalysts [21]. Several approaches for the preparation of Pt catalysts on a magnetically retrievable phase have been reported, including a Pt-based magnetically separable catalyst ( $\text{Pt/SiO}_2/\text{Fe}_3\text{O}_4$ ) modified with cinchonidine [22],  $\text{Fe}_3\text{O}_4/\text{SiO}_2\text{-Pt/Au/Pd}$  magnetic nanocatalysts with multifunctional hyperbranched polyglycerol amplifiers [23] and platinum impregnated on magnetite [13].

✉ Youxin Li  
lyx@tju.edu.cn

<sup>1</sup> Tianjin Key Laboratory for Modern Drug Delivery and High-Efficiency, Collaborative Innovation Center of Chemical Science and Engineering, School of Pharmaceutical Science and Technology, Tianjin University, Tianjin 300037, China

<sup>2</sup> School of Pharmaceutical Science and Technology, Tianjin University, Room 412-8, Building No. 24, 92 Weijin Road, Nankai District, Tianjin 300072, China

Nevertheless, a number of drawbacks remain, including high manufacturing costs, poor stability and aggregation to platinum clusters resulting in undesired side reactions, such as isomerization and hydrogenation [24–26].

In this paper, we report on our efforts to prepare four magnetic heterogeneous Pt catalysts based on magnetic silica nanoparticles with boronic, nitric, sulfuric or carboxylic acid groups, designated as  $\text{Fe}_3\text{O}_4@\text{SiO}_2\text{-BA@Pt}$ ,  $\text{Fe}_3\text{O}_4@\text{SiO}_2\text{-NA@Pt}$ ,  $\text{Fe}_3\text{O}_4@\text{SiO}_2\text{-SA@Pt}$  and  $\text{Fe}_3\text{O}_4@\text{SiO}_2\text{-CA@Pt}$ , respectively. To the best of our knowledge, there are no previous reports of magnetic heterogeneous Pt catalysts immobilized through these acid groups, except for carboxylic acids as reported by our group [27, 28]. After characterizing the four Pt catalysts, their catalytic stabilities and activities were investigated. The Pt catalyst immobilized through boronic acid proved to be most promising and was further used to catalyze hydrosilylation of a range of alkenes and alkynes as substrates, and methyldichlorosilane or triethoxysilane as silanes.

## Experimental section

### Reagents and chemicals

Unless otherwise stated, all chemicals were of analytical grade or better.  $\text{FeSO}_4 \cdot 7\text{H}_2\text{O}$  (> 99%) was purchased from Tianjin Jiezheng Chemical Trade Co. (Tianjin, China).  $\text{Fe}_2(\text{SO}_4)_3$  (> 99%) was obtained from Tianjin Yuanli Chemical Co. (Tianjin, China). Ammonium hydroxide (28%, w/w), sodium silicate, hydrochloric acid and methanol were purchased from Tianjin Kemiou Chemical Reagent Co. (Tianjin, China). 3-Glycidyloxypropyltrimethoxysilane (GPTMS) was obtained from Shanghai Macklin Biochemical Co. (Shanghai, China). 3-Nitroaniline, 3-aminophenylboronic acid monohydrate, 3-aminophenylsulfonic acid and 4-aminobenzoic acid were purchased from Shanghai Bid pharmatech Ltd. (Shanghai, China). Chloroplatinic acid ( $\text{H}_2\text{PtCl}_6 \cdot 6\text{H}_2\text{O}$ ) was purchased from Tianjin Fengchuan Chemical Reagent Technologies Co. (Tianjin, China). Triethoxysilane and methyldichlorosilane were obtained from Zhejiang Kaihua Synthetic Co. (Zhejiang, China). 1-Hexene was obtained from Shanghai Aladdin Biological Technology Co. (Shanghai, China). 1-Hexyl-methyldichlorosilane was purchased from CNW Technologies Co. (Germany). Allyl glycidyl ether, styrene and 5-hexen-2-one were obtained from Ninedinn chemistry Co. (Shanghai, China). Diphenylacetylene, trans- $\beta$ -methylstyrene,  $\alpha$ -methylstyrene, 1-phenyl-1-butyne, allylbenzene, 4-phenyl-1-butene, phenylacetylene and (E)-4-phenyl-3-buten-2-one were purchased from Beijing Ouhe Technology Co. (Beijing, China). Platinum standard solution was purchased from Beijing Beina Chuanglian Biotechnology Institute (Beijing, China). Distilled water was supplied

by Yongyuan Distilled Water Manufacturing Centre (Tianjin, China). All other reagents were obtained from Tianjin Jiangtian Chemical Technology Co. (Tianjin, China).

### Instrumentation

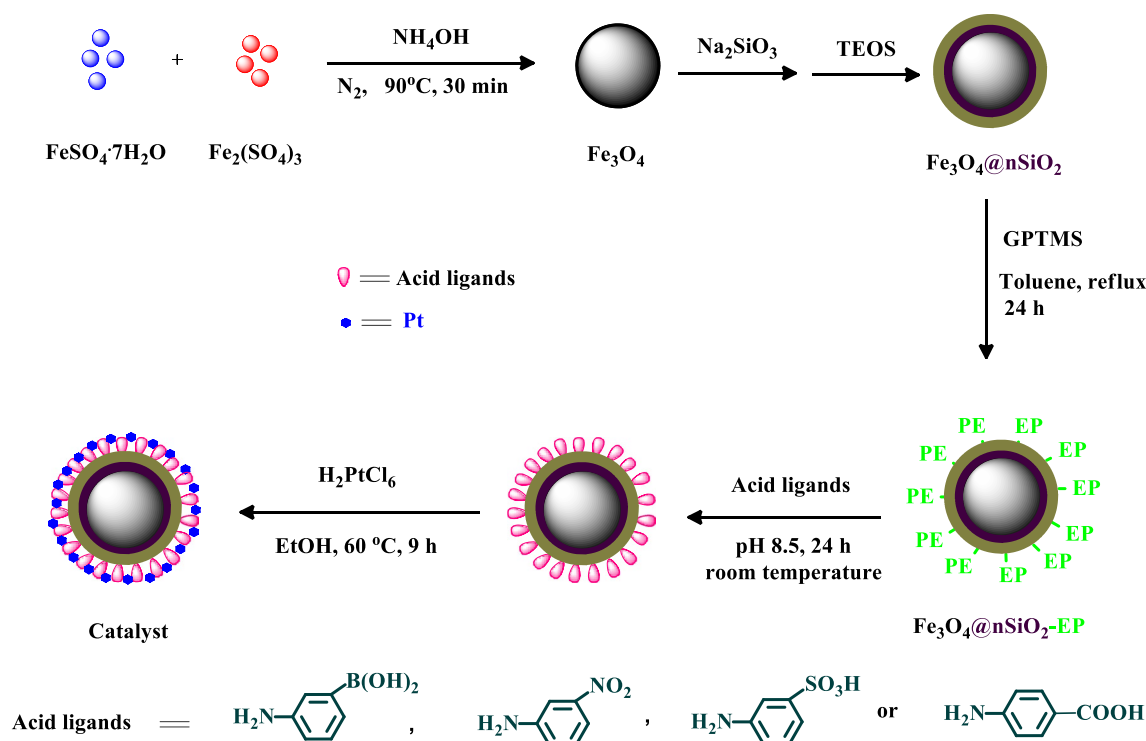
Pt contents of these materials were assayed with a HITACHI 180-80 polarized Zeeman atomic absorption spectrophotometer (AAS) (HITACHI, Ltd., Japan). Particle morphology was investigated using a Hitachi S2800 scanning electron microscope (SEM) and a JEM-2100HR (JEOL, Japan) transmission electron microscope (TEM) operating at an accelerating voltage of 200 kV. X-ray diffraction analysis (XRD) results were obtained on a D/MAX-2500 X-ray diffractometer (Rigaku Corporation, Japan), using Cu  $K\alpha$  radiation, operated at 40 kV, 30 mA and room temperature. X-ray photoelectron spectroscopy (XPS) data were obtained under ultrahigh vacuum ( $1 \times 10^{-8}$  Pa) on an UIVAC-PHI 1600 ESCA spectrometer with an Al anode (Al  $K\alpha = 1486.6$  eV). Ultraviolet–visible (UV–Vis) absorption spectra were obtained with a U-3900 ultraviolet–visible spectrophotometer (Hitachi, Japan). Gas chromatography was carried out with a GC2020 chromatograph equipped with a 30 m capillary column with a stationary phase of 5% phenyl–95% methyl polysiloxane, under the following conditions: initial temperature 60 °C for 3 min; ramp 10 °C  $\text{min}^{-1}$ ; final temperature 260 °C for 5 min; injector and detector temperature 260 °C; a sample of 0.8  $\mu\text{L}$  was injected and the split ratio was 1/30. The magnetic behaviors of these materials were assayed with a vibrating sample magnetometer (VSM) LDJ-9600 (USA).

### Preparation of the catalysts

Scheme 1 illustrates the preparation of these immobilized Pt nano-catalysts.

Magnetite ( $\text{Fe}_3\text{O}_4$ ) nanoparticles were prepared by chemical coprecipitation of  $\text{Fe}^{3+}$  and  $\text{Fe}^{2+}$  in ammonium hydroxide solution, based on the reported methods [29, 30]. The surface of the  $\text{Fe}_3\text{O}_4$  nanoparticles was then covered with  $\text{SiO}_2$  ( $\text{SiO}_2$  encapsulated  $\text{Fe}_3\text{O}_4$  nanoparticles,  $\text{Fe}_3\text{O}_4@\text{SiO}_2$ ) according to the published method [31].

To prepare epoxy propyl modified  $\text{Fe}_3\text{O}_4@\text{SiO}_2$  ( $\text{Fe}_3\text{O}_4@\text{SiO}_2\text{-EP}$ ), a dispersion of  $\text{Fe}_3\text{O}_4@\text{SiO}_2$  powder (500 mg) in toluene (50 mL) was ultrasonically irradiated for 20 min. After adding  $\gamma$ -glycidoxypropyltrimethoxysilane (4 mmol), the mixture was boiled at reflux under nitrogen for 24 h. The product was separated with a magnet and washed sequentially with dichloromethane (50 mL), acetone (50 mL), dichloromethane (50 mL) and diethyl ether (50 mL). Finally, the solid product was dried under vacuum at 80 °C overnight.



**Scheme 1** Synthesis of four immobilized Pt nano-catalysts on magnetic silica nanoparticles through boronic acid, nitric acid, sulfuric acid or carboxylic acid groups

Next, 3-aminophenylboronic acid monohydrate (APBA·H<sub>2</sub>O, 1.012 g), 3-nitroaniline (1.1064 g), 3-aminophenylsulfonic acid (1.3079 g) or 4-aminobenzoic acid (1.2456 g) were each dissolved in deionized water (100 mL). A portion of Fe<sub>3</sub>O<sub>4</sub>@SiO<sub>2</sub>-EP (1.0 g) was added to each solution and dispersed by ultrasonic irradiation. After adjusting the pH to 8.5 using NaOH solution, the mixture was mechanically stirred for 24 h at room temperature. Each product was then separated, washed and dried as described above.

Finally, a solution of H<sub>2</sub>PtCl<sub>6</sub>·6H<sub>2</sub>O (0.2 g) in ethanol (10 mL) was mixed with a portion of the acid-derivatized nanoparticles (1.0 g) and the mixture was vigorously stirred for 9 h at 60 °C under nitrogen. The resulting catalysts (Fe<sub>3</sub>O<sub>4</sub>@SiO<sub>2</sub>-BA@Pt, Fe<sub>3</sub>O<sub>4</sub>@SiO<sub>2</sub>-NA@Pt, Fe<sub>3</sub>O<sub>4</sub>@SiO<sub>2</sub>-SA@Pt and Fe<sub>3</sub>O<sub>4</sub>@SiO<sub>2</sub>-CA@Pt) were magnetically separated, washed with deionized water (3 times) and ethanol (3 times) and dried under vacuum at 80 °C overnight.

### Catalytic hydrosilylation reactions

All catalytic reactions were performed without nitrogen protection. A portion of the catalyst and 10 mmol of the alkene/alkyne were placed in a 10 mL flat-bottomed tube equipped with a reflux condenser, and the mixture was stirred 30 min at 60 °C. After adding 15 mmol of the

required silane, the mixture was continually heated and stirred for a certain time, then cooled to room temperature. The catalyst was separated with an external magnet, and the solution was assayed by GC using n-decane as an internal standard.

## Results and discussion

### Preparation of the heterogeneous catalysts

It is well known that anions such as boronate, nitrate, sulfate and carboxylate can interact with Pt cations by ionic attraction. Such interactions are highly dependent on the pH and ionic strength of solution, often making it difficult to immobilize platinum ions. Moreover, these anions will not attract other negatively charged species such as PtCl<sub>6</sub><sup>2-</sup>. Hence, research to date has focused on heterocyclic supports or materials such as TiO<sub>2</sub> and Al<sub>2</sub>O<sub>3</sub> [32–34]. Following our discovery that carboxylic acids can immobilize platinum catalysts through coordination interactions [27, 28], we have investigated the feasibility of immobilizing Pt salts through coordination interactions with boronic, nitric or sulfuric acids. For comparison, carboxylic acid-modified magnetic silica gel was also used to immobilize Pt.

## Catalyst characterization

The surface morphology and size of the Pt-containing nanoparticles were characterized using TEM (Fig. 1a–d). The images showed that the average particle size was 10–20 nm, within the range for nanoparticles. Furthermore, the micrographs showed a spherical shape for these materials, while dry powder images showed aggregation of the nanoparticles. To avoid damage to the TEM instrument, high-resolution TEM images of these materials were not obtained. In aqueous suspension, all four samples appeared uniform and mono-dispersed. Figure 1e shows a typical image.

The quantities of Pt in these materials were assayed by AAS, and the results are shown in Table 1. The

$\text{Fe}_3\text{O}_4@\text{SiO}_2\text{-BA}$  could immobilize 0.174 mmol/g Pt (33.95 mg/g), about three times as much as  $\text{Fe}_3\text{O}_4@\text{SiO}_2\text{-NA}$  (0.055 mmol/g Pt) and five times as much as  $\text{Fe}_3\text{O}_4@\text{SiO}_2\text{-CA}$  (0.032 mmol/g). Contrary to our expectations, we found no detectable Pt on the sulfate-based  $\text{Fe}_3\text{O}_4@\text{SiO}_2\text{-SA}$  support. Previous reports have shown that the  $-\text{B}(\text{OH})_2$  group can form a stable ring with cis-diols [35]. Thus, we guess that the  $-\text{B}(\text{OH})_2$  group can form a chelate ring with Pt to anchor so much Pt catalyst.

The wide-angle XRD patterns of these catalysts are shown in Fig. 2a. Almost identical XRD patterns were obtained for  $\text{Fe}_3\text{O}_4@\text{SiO}_2\text{-BA@Pt}$ ,  $\text{Fe}_3\text{O}_4@\text{SiO}_2\text{-NA@Pt}$ ,  $\text{Fe}_3\text{O}_4@\text{SiO}_2\text{-CA@Pt}$  and  $\text{Fe}_3\text{O}_4@\text{SiO}_2\text{-SA@Pt}$  compared with  $\text{Fe}_3\text{O}_4$ . Characteristic diffraction peaks were observed

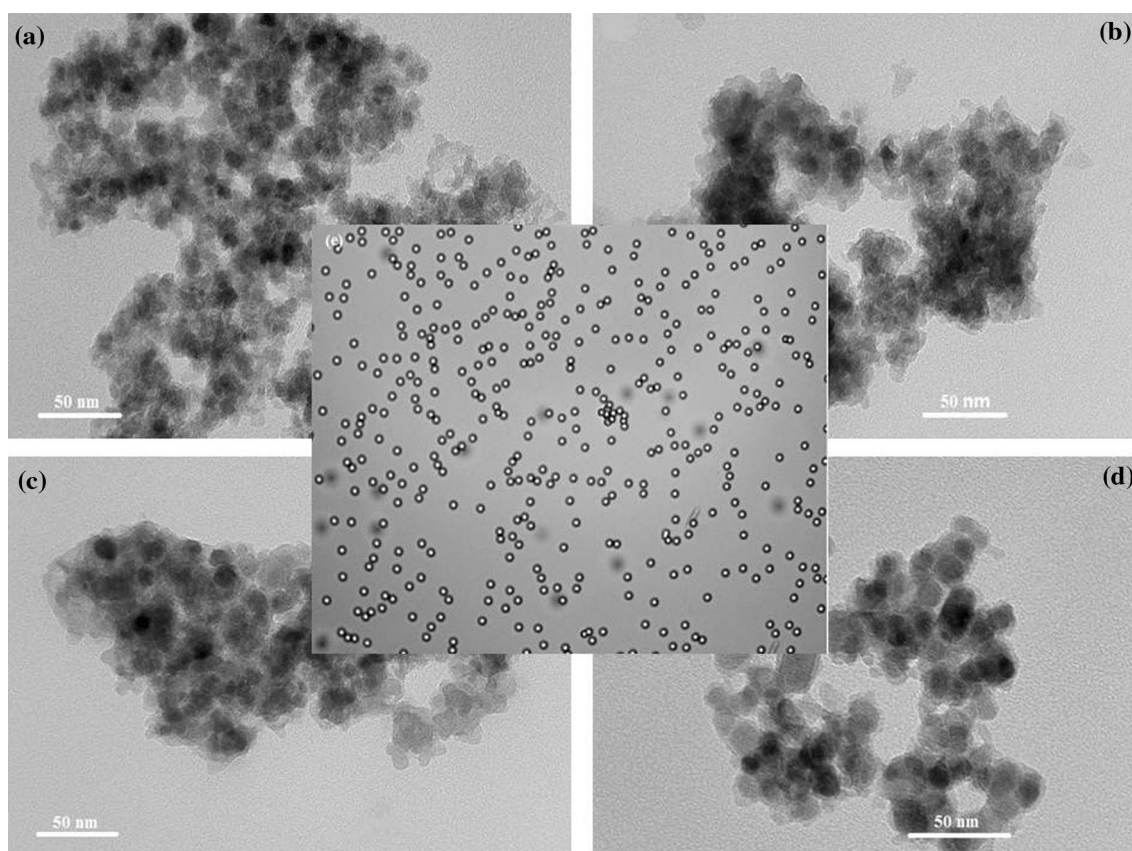


**Fig. 1** TEM micrograph of **a**  $\text{Fe}_3\text{O}_4@\text{SiO}_2\text{-BA@Pt}$ , **b**  $\text{Fe}_3\text{O}_4@\text{SiO}_2\text{-NA@Pt}$ , **c**  $\text{Fe}_3\text{O}_4@\text{SiO}_2\text{-CA@Pt}$ , **d**  $\text{Fe}_3\text{O}_4@\text{SiO}_2\text{-SA@Pt}$  and **e** microscopic observation of the synthetic magnetic material dispersed in water

**Table 1** The amount and valence state of Pt on functional magnetic nanoparticles

Entry	Catalyst	AAS results		XPS analysis		
		Pt ( $\text{mg g}^{-1}$ )	Pt ( $\text{mmol g}^{-1}$ )	Pt <sup>4+</sup> (%)	Pt <sup>2+</sup> (%)	Pt <sup>0</sup> (%)
1	$\text{Fe}_3\text{O}_4@\text{SiO}_2\text{-BA@Pt}$	33.95	0.174	30.07	42.41	27.52
2	$\text{Fe}_3\text{O}_4@\text{SiO}_2\text{-NA@Pt}$	10.76	0.055	6.02	87.63	6.35
3	$\text{Fe}_3\text{O}_4@\text{SiO}_2\text{-CA@Pt}$	6.32	0.032	29.09	48.02	22.89
4	$\text{Fe}_3\text{O}_4@\text{SiO}_2\text{-SA@Pt}$	–	–	–	–	–



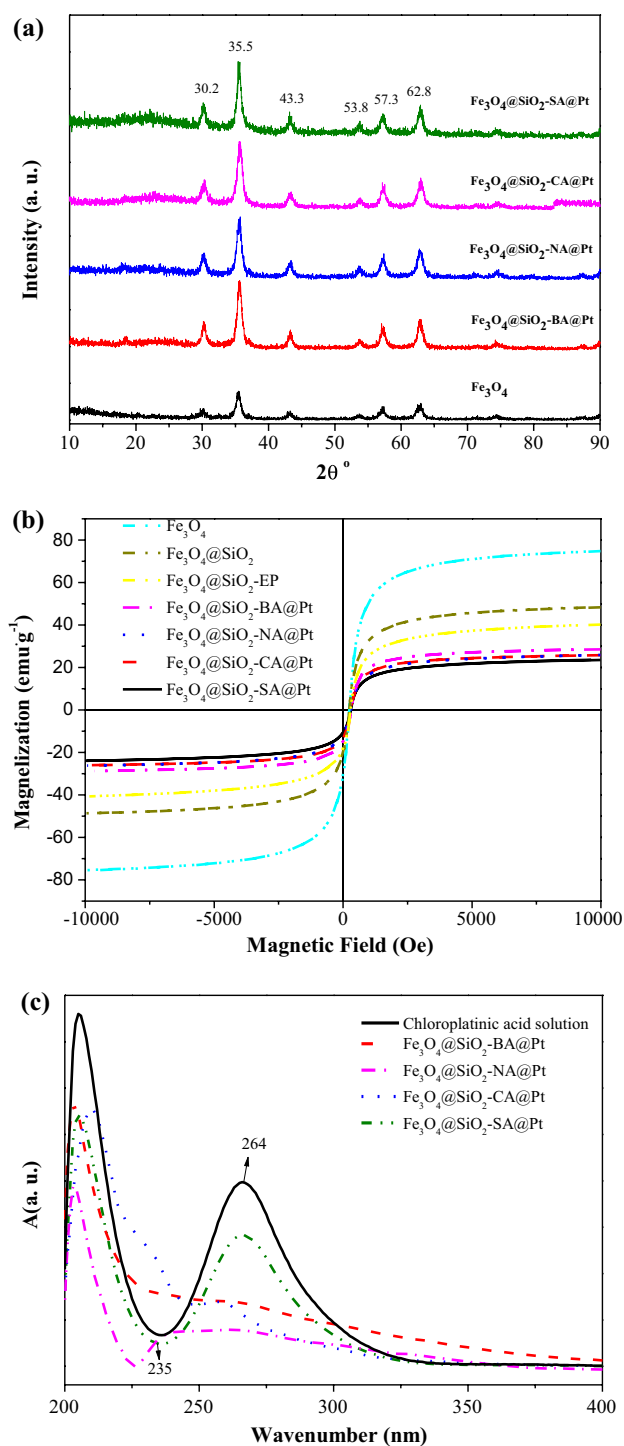


**Fig. 2** **a** XRD patterns of  $\text{Fe}_3\text{O}_4$ ,  $\text{Fe}_3\text{O}_4@SiO_2\text{-BA@Pt}$ ,  $\text{Fe}_3\text{O}_4@SiO_2\text{-NA@Pt}$ ,  $\text{Fe}_3\text{O}_4@SiO_2\text{-CA@Pt}$  and  $\text{Fe}_3\text{O}_4@SiO_2\text{-SA@Pt}$ . **b** Room temperature magnetization curves of  $\text{Fe}_3\text{O}_4$ ,  $\text{Fe}_3\text{O}_4@SiO_2$ ,  $\text{Fe}_3\text{O}_4@SiO_2\text{-EP}$ ,  $\text{Fe}_3\text{O}_4@SiO_2\text{-BA@Pt}$ ,  $\text{Fe}_3\text{O}_4@SiO_2\text{-NA@Pt}$ ,  $\text{Fe}_3\text{O}_4@SiO_2\text{-CA@Pt}$  and  $\text{Fe}_3\text{O}_4@SiO_2\text{-SA@Pt}$ . **c** The UV absorption curves of the chloroplatinic acid solution before and after immobilization

at  $2\theta$  of  $30.2^\circ$ ,  $35.5^\circ$ ,  $43.3^\circ$ ,  $53.8^\circ$ ,  $57.3^\circ$  and  $62.8^\circ$ , corresponding to the (220), (311), (400), (422), (511) and (440) diffraction planes of  $\text{Fe}_3\text{O}_4$ , respectively. These peaks match with the magnetic cubic structure of  $\text{Fe}_3\text{O}_4$  (JCPDS 65-3107) [36]. No obvious  $\text{SiO}_2$  peaks were observed in the XRD patterns, indicating the amorphous nature of the  $\text{SiO}_2$  coating. No obvious peaks of metallic Pt were detected, indicating that the amount of Pt was too low and/or the Pt particles were highly dispersed on these supports.

The Scherrer formula was used to calculate the crystallite size of these materials [37, 38]:

$$D = \frac{K\lambda}{\beta \cos \theta}$$

where  $D$  is the crystallite size (nm),  $\lambda$  is the X-ray wavelength ( $k = 1.542 \text{ \AA}$ ) ( $\text{Cu}_{k\alpha}$ ),  $\beta$  is the full width at half-maximum height (FWHM) of the line,  $K$  is the Scherrer constant ( $K = 0.94$ ) [39], and  $\theta$  is the Bragg diffraction angle ( $^\circ$ ). As can be seen, the four immobilized catalysts ( $\text{Fe}_3\text{O}_4@SiO_2\text{-BA@Pt}$ ,  $\text{Fe}_3\text{O}_4@SiO_2\text{-NA@Pt}$ ,  $\text{Fe}_3\text{O}_4@SiO_2\text{-CA@Pt}$  and  $\text{Fe}_3\text{O}_4@SiO_2\text{-SA@Pt}$ ) exhibited higher crystallite size than that of  $\text{Fe}_3\text{O}_4$ . This phenomenon is most likely due to introduction of the  $\text{SiO}_2$  shell and functional groups. It also could be the result of aggregation of the materials after drying under vacuum at  $80^\circ\text{C}$  overnight followed by fine grinding in a mortar by hand [40].

The magnetic properties of the catalysts were investigated on a VSM in an applied magnetic field from  $-10,000$  to  $10,000$  Oe. The hysteresis loops of  $\text{Fe}_3\text{O}_4$ ,  $\text{Fe}_3\text{O}_4@SiO_2$ ,  $\text{Fe}_3\text{O}_4@SiO_2\text{-EP}$ ,  $\text{Fe}_3\text{O}_4@SiO_2\text{-BA@Pt}$ ,  $\text{Fe}_3\text{O}_4@SiO_2\text{-NA@Pt}$ ,  $\text{Fe}_3\text{O}_4@SiO_2\text{-SA@Pt}$  and  $\text{Fe}_3\text{O}_4@SiO_2\text{-CA@Pt}$  are shown in Fig. 2b. The saturated magnetization decreases systematically due to the surface coating of the  $\text{Fe}_3\text{O}_4$  nanoparticles with silica [41], consistent with the TEM results (Fig. 1). The magnetization saturations of the catalysts were about  $22.0 \text{ emu g}^{-1}$  such that they could easily be separated from solution with a magnet.

UV spectrometry was used to characterize the solution before and after immobilizing Pt on these acid-modified nanoparticles. The UV absorption curves (Fig. 2c) showed a maximum at  $264 \text{ nm}$  for the original chloroplatinic acid solution, corresponding to  $\text{Pt}^{4+}$  [42]. After preparation of  $\text{Fe}_3\text{O}_4@SiO_2\text{-BA@Pt}$  and  $\text{Fe}_3\text{O}_4@SiO_2\text{-CA@Pt}$ , this peak was significantly decreased, and a new peak was observed at  $235 \text{ nm}$ , corresponding to  $\text{Pt}^{2+}$  [43]. Similarly, after preparation of  $\text{Fe}_3\text{O}_4@SiO_2\text{-NA@Pt}$ , the peak at  $264 \text{ nm}$  was dramatically decreased and a new peak at  $235 \text{ nm}$  and a minimum at  $225 \text{ nm}$  indicated that most of the  $\text{Pt}^{4+}$  was changed to  $\text{Pt}^{2+}$  or  $\text{Pt}^0$ . For  $\text{Fe}_3\text{O}_4@SiO_2\text{-SA@Pt}$ , the UV spectrum of the residual solution of Pt was similar to the original, indicating very little uptake of Pt.

The XPS spectrum of the  $\text{Fe}_3\text{O}_4@SiO_2\text{-BA@Pt}$  nanoparticles is shown in Fig. 3a. Peaks corresponding to O, Si, C,

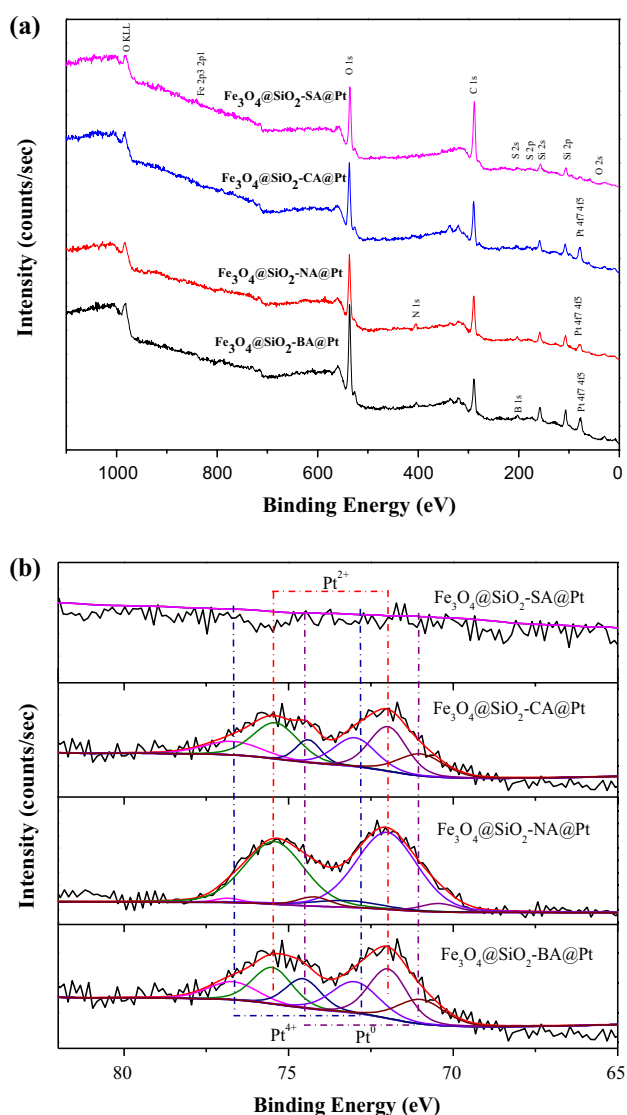


**Fig. 3** **a** XPS spectra of the elemental survey scans of  $\text{Fe}_3\text{O}_4@SiO_2\text{-BA@Pt}$ ,  $\text{Fe}_3\text{O}_4@SiO_2\text{-NA@Pt}$ ,  $\text{Fe}_3\text{O}_4@SiO_2\text{-CA@Pt}$  and  $\text{Fe}_3\text{O}_4@SiO_2\text{-SA@Pt}$ . **b** XPS spectra of the  $\text{Fe}_3\text{O}_4@SiO_2\text{-BA@Pt}$ ,  $\text{Fe}_3\text{O}_4@SiO_2\text{-NA@Pt}$ ,  $\text{Fe}_3\text{O}_4@SiO_2\text{-CA@Pt}$  and  $\text{Fe}_3\text{O}_4@SiO_2\text{-SA@Pt}$  showing Pt 4f<sub>5/2</sub> and Pt 4f<sub>7/2</sub> binding energies

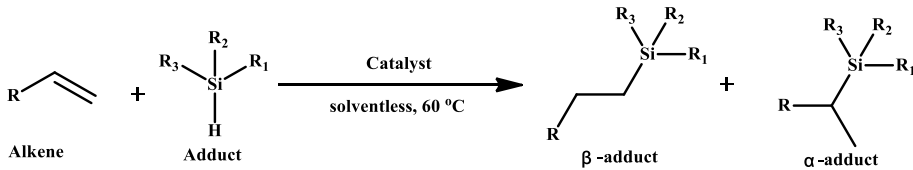
B, Pt and Fe were observed. The peaks from Si 2s (157.9 eV) and Si 2p (108.2 eV) indicated that the silica layer had been successfully coated onto the  $\text{Fe}_3\text{O}_4$  nanoparticles [30]. The B 1s peak (202.0 eV) verified that boronic acid groups were successfully bonded onto the surface of  $\text{Fe}_3\text{O}_4@SiO_2$ . The XPS spectrum of  $\text{Fe}_3\text{O}_4@SiO_2\text{-CA@Pt}$  showed the same elements as for  $\text{Fe}_3\text{O}_4@SiO_2\text{-BA@Pt}$ , except for B. Similarly, the XPS spectrum of  $\text{Fe}_3\text{O}_4@SiO_2\text{-NA@Pt}$  showed extra N rather than B. No Pt signals were observed for  $\text{Fe}_3\text{O}_4@SiO_2\text{-SA@Pt}$ , which further verified the failure in immobilization of Pt through the sulfate groups. The XPS data also indicated the oxidation state of Pt in these materials. In Fig. 3b, the binding energies of Pt at 75.8 and 71.4 eV

were assigned to Pt 4f<sub>5/2</sub> and Pt 4f<sub>7/2</sub>, respectively [44]. The valence states of platinum in these materials are shown in Table 1. It was found that about 30% exists in the form of Pt<sup>4+</sup> and 70% as Pt<sup>2+</sup> and Pt<sup>0</sup> in both  $\text{Fe}_3\text{O}_4@SiO_2\text{-BA@Pt}$  and  $\text{Fe}_3\text{O}_4@SiO_2\text{-CA@Pt}$ . In  $\text{Fe}_3\text{O}_4@SiO_2\text{-NA@Pt}$ , more than 90% is in the form of Pt<sup>2+</sup> and Pt<sup>0</sup>, which might be formed through passivation processes during preparation of the catalyst [45]. Overall, these observations confirm that Pt nanoparticles were successfully immobilized on the surfaces of  $\text{Fe}_3\text{O}_4@SiO_2\text{-BA@Pt}$ ,  $\text{Fe}_3\text{O}_4@SiO_2\text{-NA@Pt}$ , and  $\text{Fe}_3\text{O}_4@SiO_2\text{-CA@Pt}$ .

## Catalytic performance

The catalytic activities of the nanoparticles were tested for the hydrosilylation of 1-hexene with methylchlorosilane, and the results were compared with those obtained for Speier's catalyst. The results of these experiments are summarized in Table 2. Only a little 1-hexene was observed for  $\text{Fe}_3\text{O}_4@SiO_2\text{-BA@Pt}$  (0.5%) and Speier's catalyst (1.6%). Meanwhile, the proportion of the  $\beta$ -adduct, 1-hexyl-methylchlorosilane, was 98.4% for  $\text{Fe}_3\text{O}_4@SiO_2\text{-BA@Pt}$  which was significantly higher than for Speier's catalyst (78.5%).  $\text{Fe}_3\text{O}_4@SiO_2\text{-NA@Pt}$  and  $\text{Fe}_3\text{O}_4@SiO_2\text{-CA@Pt}$  also showed good selectivity (98.2 and 99.0%, respectively), together with good conversion (80.4 and 75.4%, respectively). For  $\text{Fe}_3\text{O}_4@SiO_2@Pt$  (immobilizing Pt on  $\text{Fe}_3\text{O}_4@SiO_2$ ) and  $\text{Fe}_3\text{O}_4@SiO_2\text{-EP@Pt}$ , some 1-hexene was converted, but the conversion ratios were low and the selectivities were poor. Compared with Speier's catalyst ( $6.2 \times 10^3$ ), the turnover frequencies (TOF) for 1-hexene were good for  $\text{Fe}_3\text{O}_4@SiO_2\text{-BA@Pt}$  ( $9.3 \times 10^3$ ),  $\text{Fe}_3\text{O}_4@SiO_2\text{-NA@Pt}$  ( $8.9 \times 10^3$ ) and  $\text{Fe}_3\text{O}_4@SiO_2\text{-CA@Pt}$  ( $7.3 \times 10^3$ ). In addition, we increased the amount of reactants in order to obtain the turnover number (TON). The reaction of 1-hexene (120 mmol) with methylchlorosilane (192 mmol) was catalyzed using 0.3 mg of  $\text{Fe}_3\text{O}_4@SiO_2\text{-BA@Pt}$  (0.052  $\mu\text{mol}$  Pt),  $\text{Fe}_3\text{O}_4@SiO_2\text{-NA@Pt}$  (0.016  $\mu\text{mol}$  Pt) or  $\text{Fe}_3\text{O}_4@SiO_2\text{-CA@Pt}$  (0.010  $\mu\text{mol}$  Pt) at 12 h. Under these conditions, the regioselectivity was still around 99%, while TON was up to  $1.67 \times 10^6$  for  $\text{Fe}_3\text{O}_4@SiO_2\text{-BA@Pt}$ ,  $1.23 \times 10^6$  for  $\text{Fe}_3\text{O}_4@SiO_2\text{-NA@Pt}$  and  $7.29 \times 10^5$  for  $\text{Fe}_3\text{O}_4@SiO_2\text{-CA@Pt}$ .

The catalytic activities of these nanoparticles were also tested for the hydrosilylation of styrene with methylchlorosilane. The results are summarized in Table 2 and are similar to those for hydrosilylation of 1-hexene. When  $\text{Fe}_3\text{O}_4@SiO_2\text{-BA@Pt}$  was used as catalyst, the substrates were completely converted with highest TOF. Lower yields were obtained with  $\text{Fe}_3\text{O}_4@SiO_2\text{-NA@Pt}$  (84.5%) and  $\text{Fe}_3\text{O}_4@SiO_2\text{-CA@Pt}$  (65.5%), which was similar to Speier's catalyst (68.1%). We also increased the amount of styrene (130 mmol) and methylchlorosilane (192 mmol) to allow for calculation of TON, giving values of  $1.09 \times 10^6$  for

**Table 2** Hydrosilylation of 1-hexene/styrene and methylchlorosilane catalyzed by various catalysts


Entry	Catalyst	Conversion rate (%)		Selectivity ( $\beta/\alpha$ )		TOF ( $10^3 \text{ h}^{-1}$ )	
		<i>a</i>	<i>b</i>	<i>a</i>	<i>b</i>	<i>a</i>	<i>b</i>
1	Speier's catalyst	98.4	68.1	78:22	55:45	6.2	3.5
2	$\text{Fe}_3\text{O}_4@\text{SiO}_2@\text{Pt}$	48.4	37.4	68:32	60:40	0.8	0.2
3	$\text{Fe}_3\text{O}_4@\text{SiO}_2\text{-EP}@\text{Pt}$	76.5	51.1	80:20	60:40	4.5	2.2
4	$\text{Fe}_3\text{O}_4@\text{SiO}_2\text{-BA}@\text{Pt}$	99.5	100	100:0	60:40	9.3	9.4
5	$\text{Fe}_3\text{O}_4@\text{SiO}_2\text{-NA}@\text{Pt}$	80.4	84.5	98:2	60:40	8.9	9.1
6	$\text{Fe}_3\text{O}_4@\text{SiO}_2\text{-CA}@\text{Pt}$	75.4	65.5	99:1	60:40	7.3	6.8
7	$\text{Fe}_3\text{O}_4@\text{SiO}_2\text{-SA}@\text{Pt}$	–	–	–	–	–	–

*a*: Hydrosilylation of 1-hexene and methylchlorosilane. *b*: hydrosilylation of styrene and methylchlorosilane. Reaction conditions: 10.0 mmol 1-hexene/styrene, 15 mmol methylchlorosilane, temperature: 60 °C, reaction time: 4 h, the mol ratio of Pt to 1-hexene/styrene: 1:10,000. TOF was calculated by moles of product per molar Pt per hour

0.3 mg  $\text{Fe}_3\text{O}_4@\text{SiO}_2\text{-BA}@\text{Pt}$  (0.052  $\mu\text{mol}$  Pt),  $8.21 \times 10^5$  for 0.3 mg  $\text{Fe}_3\text{O}_4@\text{SiO}_2\text{-NA}@\text{Pt}$  (0.016  $\mu\text{mol}$  Pt) and  $7.43 \times 10^5$  for 0.3 mg  $\text{Fe}_3\text{O}_4@\text{SiO}_2\text{-CA}@\text{Pt}$  (0.010  $\mu\text{mol}$  Pt) after 12 h. Hence,  $\text{Fe}_3\text{O}_4@\text{SiO}_2\text{-BA}@\text{Pt}$  shows the best performance, with significant catalytic ability and selectivity.

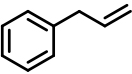
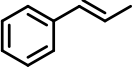
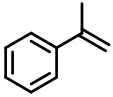
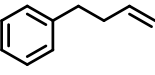
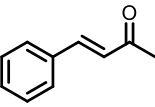
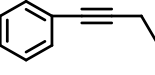
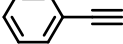
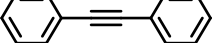
As the most effective catalyst,  $\text{Fe}_3\text{O}_4@\text{SiO}_2\text{-BA}@\text{Pt}$  was investigated further. To examine the substrate scope of  $\text{Fe}_3\text{O}_4@\text{SiO}_2\text{-BA}@\text{Pt}$ , we employed eight aromatic alkenes and alkynes and their hydrosilylation with methylchlorosilane was investigated. The results of these experiments are listed in Table 3. In most cases,  $\text{Fe}_3\text{O}_4@\text{SiO}_2\text{-BA}@\text{Pt}$  exhibited good catalytic activity. For phenylacetylene (entry 7), allylbenzene (entry 1) and  $\alpha$ -methylstyrene (entry 3), excellent conversion rates of 82–98% were obtained. Comparing with allylbenzene (entry 1) and 4-phenyl-1-butene (entry 4), the results suggest that the conversion rates of aromatic alkenes decreased with increasing alkyl chain length. For trans- $\beta$ -methylstyrene (entry 2), (*E*)-4-phenyl-3-buten-2-one (entry 5), 1-phenyl-1-butyne (entry 6) and diphenylacetylene (entry 8), the conversion rates of internal aromatic alkenes/alkynes were lower than for terminal aromatic alkenes/alkynes.

We also employed other alkenes to evaluate the catalytic activity and regioselectivity of  $\text{Fe}_3\text{O}_4@\text{SiO}_2\text{-BA}@\text{Pt}$ , giving the results listed in Table 4. The catalyst showed excellent performance in these reactions. The selectivity for the  $\beta$ -adduct was above 99.0% in the reaction of 1-hexene with both methylchlorosilane and triethoxysilane (entries 1 and 2). The yield of the  $\beta$ -adduct was up to 85.3% in hydrosilylation of 5-hexen-2-one and methylchlorosilane, with a conversion rate of 89.4%. When

methylchlorosilane was replaced by triethoxysilane, the selectivity for 5-hexen-2-one increased to 91.4% (entries 3 and 4). Similar selectivity (above 95.0%) for the  $\beta$ -adduct was observed in hydrosilylation of allyl glycidyl ether and methylchlorosilane or triethoxysilane (entries 5 and 6). Compared with the hydrosilylation of styrene and methylchlorosilane (yield 100%, selectivity 60%), the  $\beta$ -adduct yield for hydrosilylation of styrene and triethoxysilane was down to 56.6%, while selectivity was slightly improved to 77.8% (entry 7). These results indicate that catalysis with  $\text{Fe}_3\text{O}_4@\text{SiO}_2\text{-BA}@\text{Pt}$  gave good activity and selectivity, even when methylchlorosilane was substituted with triethoxysilane.

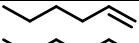
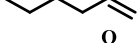
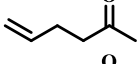
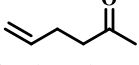
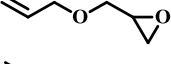
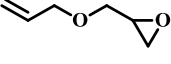
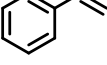
A crucial benefit regarding this magnetic catalyst is its straightforward separation; we therefore investigated the recyclability of  $\text{Fe}_3\text{O}_4@\text{SiO}_2\text{-BA}@\text{Pt}$ , using the reaction of 1-hexene with methylchlorosilane. On completion of the first reaction, the catalyst was separated with a magnet and the decantate was analyzed. Fresh substrates were then added to the recycled catalyst, and a further run was performed. In this way,  $\text{Fe}_3\text{O}_4@\text{SiO}_2\text{-BA}@\text{Pt}$  was reused eight times under the following conditions: reaction temperature 60 °C, reaction time 4 h, mole ratio between 1-hexene and saline 1:1.5, and mole ratio of Pt to 1-hexene 1:10,000. The results are shown in Table 5. The yields of 1-hexyl-methylchlorosilane were 96.5% for the first run and 95.2% for the eighth. No Pt was detected in the product solutions. The amount of Pt after the eight experiments (0.171 mmol/g) was close to the original amount (0.174 mmol/g) for  $\text{Fe}_3\text{O}_4@\text{SiO}_2\text{-BA}@\text{Pt}$ , indicating excellent stability for this catalyst.

**Table 3** Catalytic activity of  $\text{Fe}_3\text{O}_4@\text{SiO}_2\text{-BA@Pt}$  for the hydrosilylation of methylchlorosilane and aromatic alkene or alkyne

Entry	Alkene	Silane	Time/h	Conversion rate (%)
1		Methylchlorosilane	4	85
2		Methylchlorosilane	4	74
3		Methylchlorosilane	4	82
4		Methylchlorosilane	4	65
5		Methylchlorosilane	4	47
6		Methylchlorosilane	6	48
7		Methylchlorosilane	6	98
8		Methylchlorosilane	6	30

Reaction conditions: 10 mmol alkene or alkyne, 15 mmol methylchlorosilane, temperature: 60 °C, reaction time: 4 h, the mol ratio of Pt to alkene or alkyne was 1:8000

**Table 4** Hydrosilylations of alkene and methylchlorosilane or triethoxysilane

Entry	Alkene	Silane	Time (h)	Conversion rate (%)	Selectivity (%) $\beta$ -Adduct
1		Methylchlorosilane	4	98.3	>99.0
2		Triethoxysilane	4	99.4	>99.0
3		Methylchlorosilane	4	89.4	85.3
4		Triethoxysilane	4	81.2	91.4
5		Methylchlorosilane	4	96.4	>95.0
6		Triethoxysilane	4	96.8	>95.0
7		Triethoxysilane	6	77.8	56.6

Reaction conditions were same as Table 3



**Table 5** Recyclability of the Fe<sub>3</sub>O<sub>4</sub>@SiO<sub>2</sub>-BA@Pt in catalyzing the hydrosilylation of 1-hexene and methylchlorosilane

Runs	Yield (%)
1	96.5
2	98.6
3	97.3
4	93.2
5	94.5
6	91.4
7	93.5
8	95.2

## Conclusion

Four different acid ligand-modified magnetic nanoparticles were prepared under mild conditions to produce heterogeneous Pt catalysts. The preparation method was simple and used readily available reagents. Characterization showed these Pt catalysts are nanoparticles with an average size of 10–20 nm. In catalyzing hydrosilylation of alkenes and alkynes, three of these catalysts, especially Fe<sub>3</sub>O<sub>4</sub>@SiO<sub>2</sub>-BA@Pt, showed excellent activity and selectivity. This catalyst could be reused for eight consecutive runs, with similar activities and Pt contains. This nanocatalyst may be suitable for industrial applications.

**Acknowledgements** The authors are grateful for financial support from the National Natural Science foundation of China (No. 21605112).

## References

- James AA (2005) Supported metals in catalysis. Imperial College Press, London
- Kiyotomi K, Kohki E, Tomoo M, Kohsuke M (2006) Bull Chem Soc Jpn 79:981–1016
- Abu-Reziq R, Alper H, Wang D, Post ML (2006) J Am Chem Soc 128:5279–5282
- He Y, Cai C (2011) Catal Commun 12:678–683
- Polshettiwar V, Luque R, Fihri A, Zhu H, Bouhrara M, Basset JM (2011) Chem Rev 111:3036–3075
- Nasrollahzadeh M, Sajadi SM, Rostami-Vartooni A, Khalaj M (2015) J Mol Catal A Chem 396:297–303
- Baig RBN, Varma RS (2013) Chem Commun 49:752–770
- Shylesh S, Schunemann V, Thiel WR (2010) Angew Chem Int Ed 49:3428–3459
- Fang Y, Chen Y, Li X, Zhou X, Li J, Tang W, Huang J, Jin J, Ma J (2014) J Mol Catal A Chem 392:16–21
- Seo M, Kim S, Lee DW, Jeong HE, Lee KY (2016) Appl Catal A 511:87–94
- Kong Y, Tan R, Zhao L, Li C, Yin D (2013) Green Chem 15:2422–2433
- Zhu M, Diao G (2011) J Phys Chem C 115:24743–24749
- Cano R, Yus M, Ramon DJ (2012) ACS Catal 2:1070–1078
- Peng R, Li S, Sun X, Ren Q, Chen L, Fu M, Wu J, Ye D (2018) Appl Catal B 220:462–470
- Zhu S, Gao X, Zhu Y, Cui J, Zheng H, Li Y (2014) Appl Catal B 158–159:391–399
- Cui W, Xue D, Tan N, Zheng B, Jia M, Zhang W (2018) Chin J Catal 39:1534–1542
- Khan HA, Iqbal MI, Jaleel A, Abbas I, Abbas SA, Deog-jung K (2019) Int J Hydrogen Energy 22:2312–2322
- Roy AK (2007) Adv Organomet Chem 55:1–59
- Buisine O, Berthon-Gelloz G, Briere JF, Sterin S, Mignani G, Branlard P, Tinant B, Declercq JP, Marko IE (2005) Chem Commun 30:3856–3858
- Marko IE, Sterin S, Buisine O, Berthon G, Michaud G, Tinant B, Declercq JP (2004) Adv Synth Catal 346:1429–1434
- Ghorbani-Vaghei R, Hemmati S, Veisi H (2014) J Mol Catal A Chem 393:240–247
- Panella B, Vaegas A, Baiker A (2009) J Catal 261:88–93
- Zhou L, Gao C, Xu W (2010) Langmuir 26:11217–11225
- Lewis LN (1990) J Am Chem Soc 112:5998–6004
- Stein J, Lewis LN, Gao Y, Scott RA (1999) J Am Chem Soc 121:3693–3703
- Tsipis CA, Kefalidis CE (2006) Organometallics 25:1696–1706
- Li F, Li Y (2016) J Mol Catal A Chem 420:254–263
- Shao D, Li Y (2018) RSC Adv 8:20379–20393
- Ghorbani-Choghamarani A, Norouzi M (2016) Appl Organometal Chem 30:140–147
- Sun J, Dong Z, Sun X, Li P, Zhang F, Hu W, Yang H, Wang H, Li R (2013) J Mol Catal A Chem 367:46–51
- Heidari F, Hekmati M, Veisi H (2017) J Colloid Interface Sci 501:175–184
- Fuyuan R, Shengjun D, Chao C, Zhang N (2014) Catal Commun 46:1–5
- Spanu D, Recchia S, Mohajernia S, Schmuki P, Altomare M (2018) Appl Catal B 237:198–205
- Yan T, Huo Y, Liu Y, Rui Z, Ji H (2017) Appl Catal B 200:543–551
- Gomes AG, Azevedo AM, Aires-Barros MR, Prazeres DMF (2011) J Chromatogr A 1218:8629–8637
- Liu J, Zhou Y, Liu F, Liu C, Wang J, Pan Y, Xue D (2012) RSC Adv 2:2262–2265
- Dastan D (2017) Appl Phys A 123:699
- Dastan D, Londhe PU, Chaure NB (2014) J Mater Sci Mater Electron 25:3473–3479
- Nakhae M, Bahari A (2016) J Mater Sci Mater Electron 27:5899–5908
- Dastan D, Chaure N, Kartha M (2017) J Mater Sci Mater Electron 28:7784–7796
- Jacinto MJ, Santos OHCF, Jardim RF, Landers R, Rossi LM (2009) Appl Catal A 360:177–182
- Bai Y, Zhang S, Deng Y, Peng J, Li J, Hu Y, Li X, Lai G (2013) J Colloid Interface Sci 394:428–433
- Luty-Błocho M, Wojnicki M, Paclawski K, Fitzner K (2013) Chem Eng J 226:46–51
- Roth C, Goetz M, Fuess H (2001) J Appl Electrochem 31:793–798
- Nie R, Liang D, Shen L, Gao J, Chen P, Hou Z (2008) Appl Catal B 127:212–220

**Publisher's Note** Springer Nature remains neutral with regard to jurisdictional claims in published maps and institutional affiliations.